UCRL-JC-132438
PREPRINT

Scaling Supernova Hydrodynamics to the Laboratory

J. Kane, D. Arnett, B. A. Remington,
S. G. Glendinning, G. Bazen,
R. P. Drake, and B. A. Fryxell

This paper was prepared for submittal to the
American Physical Society 40th Annual Meeting of the
Division of Plasma Physics
New Orleans, LA
November 16-20, 1998

November 10, 1998

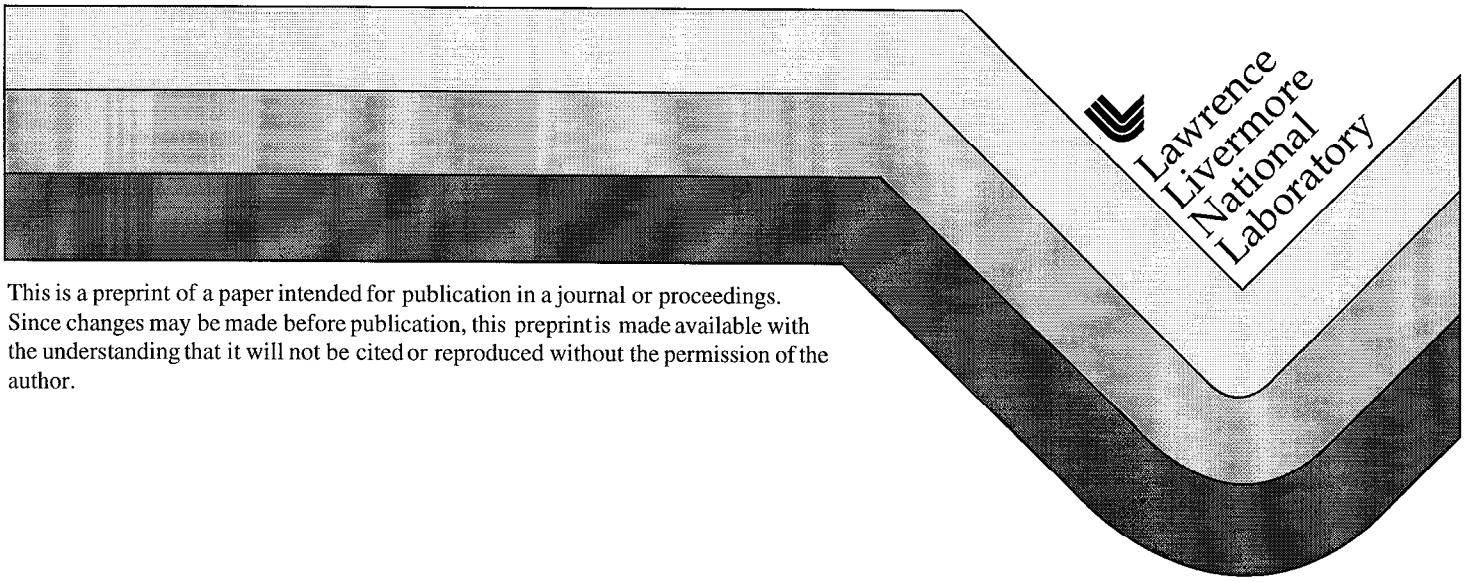

In preparation for submittal to the
Conference Proceedings of the APS DPP98 meeting,
Nov 16-20, 1998, New Orleans, LA

Scaling Supernova Hydrodynamics to the laboratory
~~Developing a laser testbed for Supernova Hydrodynamics~~

J. Kane[1] and D. Arnett[2]
University of Arizona, Tucson, AZ 85721

B. A. Remington[3], S. G. Glendinning[4], G. Bazan[5]
Lawrence Livermore National Laboratory (LLNL), Livermore CA 94550

R. P. Drake[6]
University of Michigan, Ann Arbor, MI 48109-2143

and

B. A. Fryxell[7]
NASA/GFC

[1]Mail code L-411 LLNL. jave@llnl.gov

[2]Steward Observatory. dave@bohr.as.arizona.edu

[3]L-021. remington2@llnl.gov

[4]L-021. glendinning1@llnl.gov

[6]Atmospheric Oceanic and Space Sciences, Nuclear Engineering and Radiological Sciences, 2455 Hayward St. rpdrake@umich.edu

[7]Supported by the NASA ESS HPCC Program under Grant Number NAG5-2652. fryxell@neutrino.gsfc.nasa.gov

ABSTRACT

Supernova (SN) 1987A focused attention on the critical role of hydrodynamic instabilities in the evolution of supernovae. To test the modeling of these instabilities, we are developing laboratory experiments of hydrodynamic mixing under conditions relevant to supernovae. Initial results were reported in [1]. The Nova laser is used to generate a 10-15 Mbar shock at the interface of a two-layer planar target, which triggers perturbation growth, due to the Richtmyer-Meshkov instability, and to the Rayleigh-Taylor instability as the interface decelerates. This resembles the hydrodynamics of the He-H interface of a Type II supernova at intermediate times, up to a few $\times 10^3$ s. The experiment is modeled using the hydrodynamics codes HYADES and CALE, and the supernova code PROMETHEUS. Results of the experiments and simulations are presented. Analysis of the spike bubble velocities using potential flow theory and Ott thin shell theory is presented, as well as a study of 2D vs. 3D difference in growth at the He-H interface of SN 1987A. The scaling of hydro on microscopic laser scales to hydro on the SN-size scales is presented.

1. Introduction

Observations of SN1987A, a core collapse supernova (SN) in the Large Magellanic Cloud, strongly suggested the occurrence of material mixing driven by the Richtmyer-Meshkov (RM) and Rayleigh-Taylor (RT) instabilities [2, 3, 4, 5, 6]. The 'Bochum event' [7, 8, 9], and early detection of radioactive ^{56}Co from the explosively burned oxygen layer implied that the ^{56}Co had been mixed well into the outer layers. Doppler broadening of the gamma-ray and optical lines from ^{56}Co implied velocities in excess of 3000 km/s [10, 11, 12], whereas 2D modeling to date predicts maximum velocities of $\leq$ 2000 km/s, suggesting that perhaps 3D hydro effects should be considered. Given the fundamental role played by the RM and RT instabilities in SN evolution, it is desirable to develop the means of testing the hydrodynamics of the SN codes. We report here on experiments using the Nova laser at Lawrence Livermore National Laboratory (LLNL) to test the modeling of compressible RM and RT instabilities at relevant pressures. We use the SN code PROMETHEUS to model the experiment, and for comparison, the LLNL code CALE. We also present an analysis of the hydrodynamic growth in the experiment in terms of theory for incompressible hydrodynamic instabilities, and report on numerical investigations of 2D vs. 3D hydro differences in SN 1987A.

2. 1D Simulations of SN and Laser Experiment

Fig. 1 shows a 20M$_\odot$ model for the progenitor of SN 1987A [13], and from 1D PROMETHEUS (a multi-D Piecewise Parabolic Method [PPM] hydro code), the velocity profile of the He-H interface during the explosion, and the 1D pressure and density profiles 2000 s into the explosion. For more details of the SN 1987A explosion, the PROMETHEUS code, and the simulations shown here, see [6, 14, 15, 16, 17, 1]. At the He-H interface, the strong acceleration induced by the blast wave, followed by deceleration, along with the

crossed pressure and density gradients, suggest that the He-H interface should exhibit strong RM and RT instability, with the full multi-D interface evolving well into the nonlinear regime, as seen in [14, 15, 16].

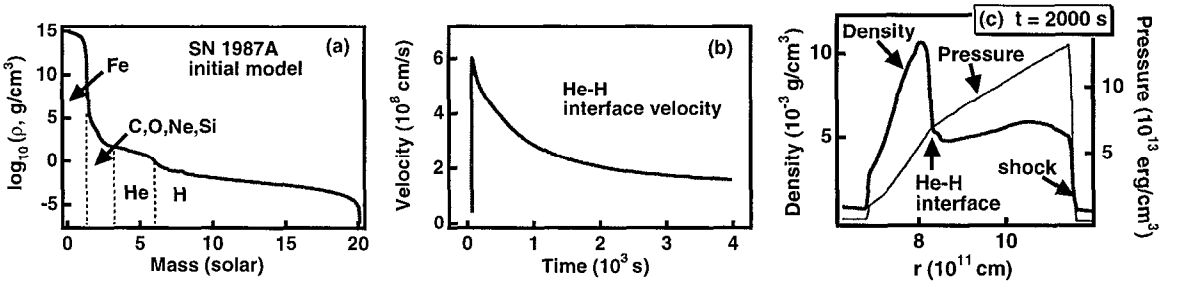

Fig. 1.— (a) Initial model for SN 1987A (b) He-H interface velocity (c) crossed density and pressure gradients at the He-H interface after passage of the shock.

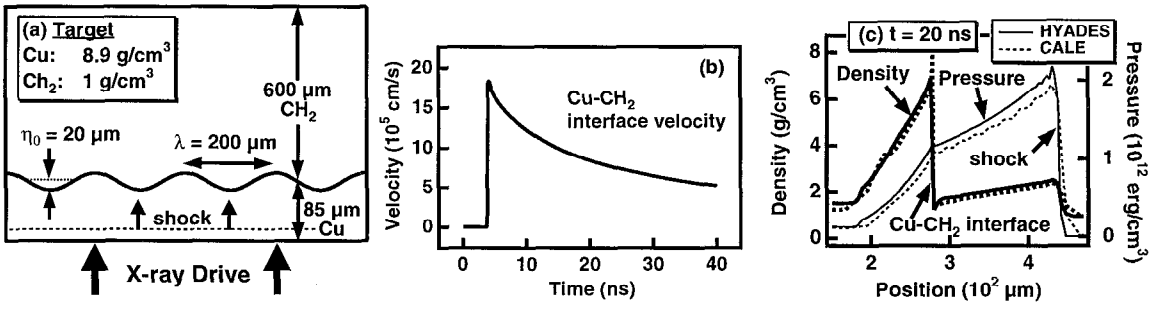

Fig. 2.— (a) Initial target for Nova experiment (b) Cu-CH_2 interface velocity (c) crossed density and pressure gradients at the Cu-CH_2 interface.

The Nova experimental configuration is illustrated in Fig. 2; for further discussion of the experiment and the experimental techniques, see [1, 18, 19, 20, 21]. The Nova laser is used to produce an X-ray drive which shocks a two-layer Cu-CH_2 planar target having an imposed material perturbation at the Cu-CH_2 interface. Figs. 2b and c show HYADES simulations of a 1D (unperturbed) experiment; as in the SN case (Fig. 1), the interface is first accelerated by the shock and then decelerated, and the pressure and density gradients are crossed at the interface; the Cu-CH_2 should also exhibit strong RM and RT instability. We typically observe the experiment for up to 40 ns.

We model the laser experiment using a combination of codes: HYADES, CALE and PROMETHEUS. The HYADES code [22] is a 1D Lagrangian code with multigroup radiation transport and tabular EOS, and CALE is a 2D Arbitrary Lagrangian Eulerian (ALE) code [23] with tabular EOS and interface tracking. PROMETHEUS was described above. Ideal gas EOS is used for all the PROMETHEUS simulations of the laser experiments. We use the measured x-ray radiation temperature, $T_r(t)$, as the energy input to HYADES, and the versions of CALE and PROMETHEUS that we are using do not have radiation transport. We begin all simulations using HYADES, then map to PROMETHEUS and CALE at 2.45 ns, just prior to the arrival of the shock at the thinnest part of the (perturbed) Cu. As seen in Fig. 2c, CALE and HYADES agree well long after the mapping, indicating that the experiment is hydro-dominated. For a discussion of scaling of hydro instability growth between the SN and Nova case, see [1, 24, 25, 26].

3. Results and 2D Simulations

Fig. 3a shows a 2D image from the experiment at $t = 33.2$ ns. The Cu-CH_2 interface shows the classic nonlinear RM/RT bubble-and-spike shape, and there are faint indications of a roll-up at the very tip of the spike. We initiate our 2D simulations in the same manner as in 1D: we map the conditions from the HYADES calculation at 2.45 ns. Fig. 3b-d show PROMETHEUS and CALE simulations of the experiment. The gross features of the experiment are well reproduced by both simulations. For further details about the data and simulations, see [1]. Fig. 4 compares spike and bubble position from the experiment, CALE, and PROMETHEUS. The observed spike and bubble fronts are well reproduced by both hydrodynamics codes. Also shown is the position of an unperturbed interface as calculated by CALE and PROMETHEUS. In [1] we presented a preliminary analysis of the hydrodynamic growth in terms of nonlinear RM and RT theory for semi-infinite fluids

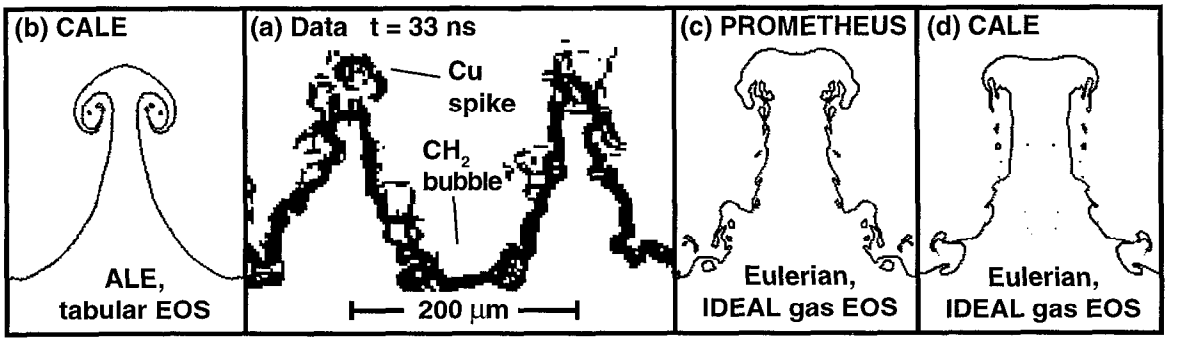

Fig. 3.— Data and simulations for 2D experiment. (a) Outline of Cu-CH_2 interface extracted from radiograph of experiment at 33 ns. (b) CALE simulation, in (ALE) mode and using tabular EOS. (c) PROMETHEUS simulation, with fixed (Eulerian) orthogonal grid and ideal gas EOS. There is more fine structure with PROMETHEUS. (d) When CALE is run with Eulerian orthogonal grid and ideal gas EOS, the result is similar to PROMETHEUS, with the fine structure somewhat supressed by the interface tracking in CALE. CALE can be started with an orthogonal or non-orthogonal grid; in the former case the initial sinusoidal interface must be stairstepped along the grid, while in the latter case the interface can be piecewise smooth. When CALE is run in 8 different ways, (initial interface:smooth/stairstepped) × (grid:Eulerian[fixed]/ALE) × (EOS:tabular/ideal), the dominant factor in producing fine structure appears to be the stairstepping (not shown.)

[27, 25, 26], and are preparing more detailed analyses for an upcoming publication. In the more detailed analyses we consider the effects of the 'accordionlike' decompression of the Cu and CH_2 layers, the effects of the time varying effective g (interface deceleration,) and the finite thickness of the dense part of the Cu layer (see. Fig. 2b.) In one of our analyses, we do a 2D simulation in which we impose a curl-free single mode velocity perturbation at a flat Cu-CH_2 interface, with the same wavelength as the perturbation in the experiment, after the shock passes the interface. We use the results of a 1D simulation to estimate the background decompression velocities everywhere in the two layers, and then subtract these velocities from the bubble and spike velocities. We then use a drag-vs.-buoyancy model [25, 26] to analyze the 'undecompressed' bubble and spike velocities. In Fig. 4b and c, we compare the 2D bubble velocity v_b to the model, and also to the the instantaneous asymptotic RT (which accounts for g) and RM (which assumes $g = 0$ after the initial impulsive accleration) velocities (see [27, 25, 26]). For the actual wavelength used in the

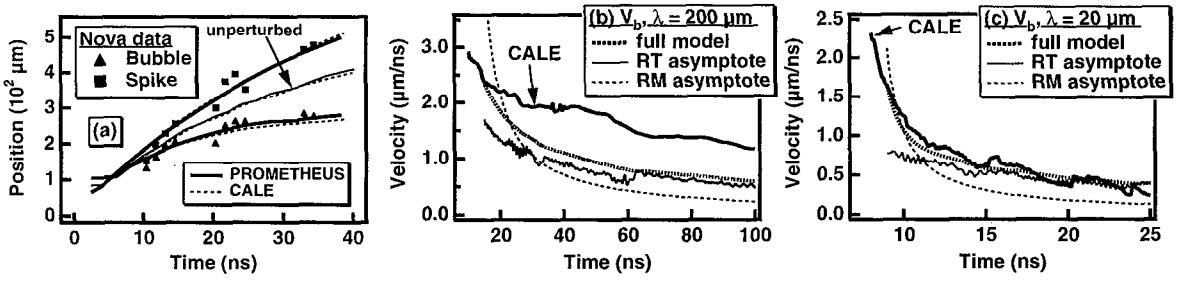

Fig. 4.— (a) Bubble and spike velocities (b) incompressible growth model vs. 'undecompressed' CALE simulation with single mode velocity perturbation, $\lambda = 200\,\mu$m (c) same for $\lambda = 20\,\mu$m

experiment, $\lambda = 200\,\mu$m, (Fig. 4b) we find that v_b does not agree well with the model, and the model does not approach either the RT or RM asymptote until well after the growth has become very nonlinear (which occurs by 60 ns.) For a smaller wavelength, $\lambda = 20\,\mu$m (Fig. 4c), we find that the v_b agrees well with the model, which quickly approaches the RT asymptote. This suggests that a large rising CH_2 bubble is able to push more easily through a dense Cu shell that is relatively thin ($\approx 35 - 70\ \mu$m) compared to the bubble dimensions ($\sim \lambda$).

Analysis of the spike velocities (not shown) suggest that the spike velocity is much harder to characterize as RM- or RT-like, possibly because of the Kelvin-Helmholtz instability at the spike tip, and because of the rapidly falling effective g, which drops as $\sim 1/t$. However, to the extent that the hydrodynamic instability growth is driven by the rising bubbles, for short wavelengths the growth seems to be RT-like. At the same time, it is clear that many complicating factors make simple classification of the growth difficult; the same is likely to be true for the SN case.

To test the idea that the Cu layer behaves as a thin shell, we next compare the undecompressed bubble growth to the growth predicted by the Ott thin shell model [xxx Ott reference.] [xxx

.. thin shell equations

]

In the same manner as [xxx ref Basko], we adapt the thin shell theory for the case where g(t), the gravitational acceleration, is inversely proportional to time. The thin shell equations in this case, and their solution, are [xxx

... $g \propto 1/t$ equations

... solution equations

]

Without justification, we modify the thin shell theory to include the postshock Atwood number A^*: [xxx

... modified thin shell equations

]

In the preceding equations A^* enters in the same manner as in the classical Rayleigh-Taylor equations for instability growth [xxx RT ref.] We use the Meyer-Blewett (MB) theory of the RM instability [xxx MB reference] to predict the amplitude and velocity of the perturbation after the shock has passed the perturbed interface, and then use the MB result as the initial conditions for the thin shell theory. The result of this analysis is shown in Fig. [Ott]. Fig. [Ott]a is a plot of undecompressed bubble and spike velocity vs. time from a 2D CALE simulation of the experiment, and the same from the result of MB mapped to the thin shell theory, for the bubble. Also shown is the result of mapping MB to drag-vs.-buoyancy potential flow theory; because the drag and buoyancy coefficients in drag-vs.-buoyancy theory assume that the growth is beyond the linear stage, we map from MB at a later time.

As seen Fig. [Ott]a, MB mapped to potential flow theory predicts the spike velocity reasonably well. The modified thin shell theory predicts the bubble velocity well at early times, while at later times the potential flow theory

predicts the bubble velocity better. In fig. [Ott]b we show the prediction of MB mapped to potential flow theory for the spike velocity minus bubble velocity; the agreeement is very good. In general, then, potential flow theory appears to describe the undecompressed peak-to-valley velocity, while a modification of the Ott thin shell theory appears to describe the bubble velocity at early times.

4. scaling

We can rigorously transform the hydrodynamic at the microscopic scale of a laser experiment to the macroscopic scale of a larger terrestrial experiment, and to the astronomical scale of a SN. In [Fig. Jacobs] we show the results of simulating the Jacobs water tank experiment [xxx ref] using CALE. Fig. [Jacobs]a shows the CALEsimulation at 0.528 s; the simulation reproduces the data in Jacobs [xxx p number, etc.] extremely well. Inf Fig. [xxx]c we compare the amplitude of the perturbation (half the bubble tip to spike tip width) from the CALE simulation to the data reported by Jacobs. The agreement is excellent, indicating that CALE is able to reproduce the post-impulse hydrodynamics in the experiment extremely well. In Fig. [xxx]d we show the result of a CALE simulation of an analogous laser-scale experiment; this experiment is a modification of our usual SN experiment — we have increased the thickness of the Cu layer so that the hydrodynamics is RM-like; the pressure behind the interface decays slowly and the initial impulse of the shock is the main factor driving the bubble and spike growth. Following [xxx Ryutov et al.] we scale the hydrodynamic quantities between the Jacobs experiment and this simulated laser experiment as follows. [

...

...

]

... Thus the time scales for growth scale between the two experiments.

Next we demonstrate a scaling from the laser experiments scale to the SN scale, as follows.

We use the transformations in the Ryutov *et al.* Ryutov *et al.* 1987 scaling paper to transform from the Jacobs and Catton water tank RT experiments Jacobs & Catton 1987. The quantity P (pressure) is somewhat mysterious in the incompressible case.

$$\nabla \cdot \vec{v} = 0 \tag{1}$$

$$\partial v/\partial t + \nabla(P/\rho) = 0 \tag{2}$$

$$\partial(P/\rho)/\partial t + \nabla(\frac{1}{2}v^2) = 0 \tag{3}$$

The quantity P is somewhat mysterious; clearly the growth of bubbles and spikes in the water tank does not depend upon the pressure, since the sound speed is 'infinite'. So I extend the scaling transformation for pressure to include an arbitrary constant 'base' pressure P_0. Then, the incompressible hydro equations are invariant under the transformation $\vec{r} = a\vec{r_1}$, $\rho = b\rho_1$, $P = c(P_1 + P_0)$, $t = dt_1$, $\vec{v} = f\vec{v_1}$, where $d = a\sqrt{b/c}$ and $f = \sqrt{c/b}$, ie.

$$t = a\sqrt{b/c}\ t_1 \tag{4}$$

$$\vec{v} = \sqrt{c/b}\ \vec{v_1} \tag{5}$$

I consider the case 'D4' of Jacobs & Catton 1987; this case is described on

p. 365 and results are shown in Fig. 9(d) on p. 367. In case D4, $g/g_0 = 10$ **and** $k = 2\pi/\lambda = 2.23$ **cm**$^{-1}$**.**

$$\rho_1 \approx 1 \text{ g/cm}^3 \tag{6}$$

$$P_1 = P_{\rm atm}\ g/g_0 + P_0 \approx 10 \times 10^6 \text{ erg/cm}^3 + P_0 \tag{7}$$

$$\lambda = 2.8 \text{ cm} \tag{8}$$

$$t_1 = 25 \text{ ms} \tag{9}$$

I consider SN 1987A at $t = 2000$ **s, as in Fig. 2 of Ryutov** *et al.* **1987. I use the density scale height defined by the He spike for the scale length, and use the pressure at the He-H interface.**

$$\rho \approx 10^{-2} \text{ g/cm}^3 \tag{10}$$

$$P \approx 7.5 \times 10^{13} \text{ erg/cm}^3 \tag{11}$$

$$L = \nabla\rho/\rho \approx 10^{11} \text{ cm} \tag{12}$$

$$\tag{13}$$

$$a = L/\lambda = 3.6 \times 10^{10} \tag{14}$$

$$b = \rho/\rho_1 = 10^{-2} \tag{15}$$

$$c = P/(P_1 + P_0) \approx P/P_1 = 7.5 \times 10^7 \tag{16}$$

Thus, the base pressure P_0 **does make a difference to the scaling, although not to the behavior of the water tank bubbles and spikes. Here, I have just assumed that** P_0/P_1 **is small. Thus,**

$$t = a\sqrt{b/c}\ t_1 = 3.2 \times 10^3 \text{ s.} \tag{17}$$

At $t = 5000$ s, the spikes in SN 1987A are about as nonlinear as the spike in Jacobs's case D4 are at 25 ms.

5. 2D vs. 3D hydro

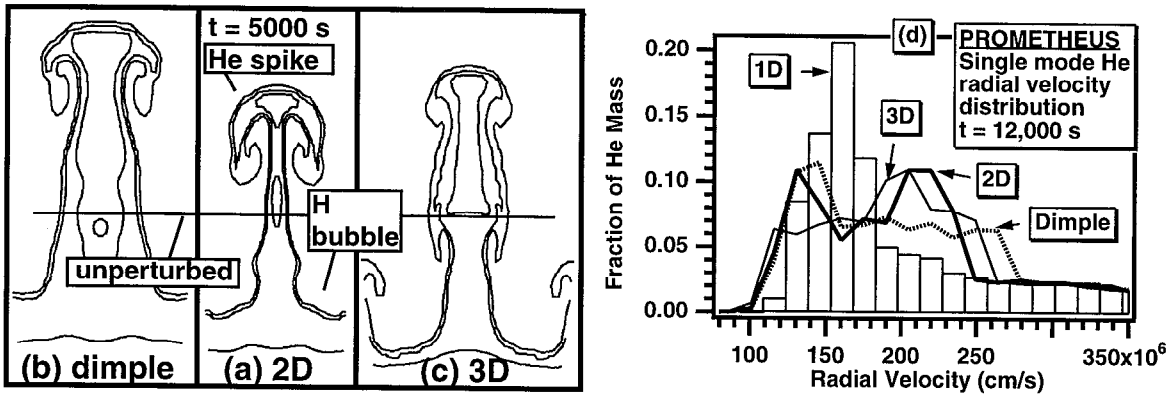

Fig. 5.— (a,b,c) He-H interface growth for 2D, dimple and 3D perturbations. (d) He velocity distributions.

We are beginning experimental investigations of 2D vs. 3D SN-relevant hydro in Nova and Omega experiments. 2D vs. 3D differences could help explain why 2D simulations of SN 1987A underpredict the observed ^{56}Co velocities. By drag-vs.-buoyancy arguments [28, 25, 26, 29], a 3D perturbation is expected to grow faster in the nonlinear regime than a 2D perturbation of the same wave number; perturbation of the same wave number and amplitude grow at the same rate in the linear regime [27, 25, 29]. We are currently investigating both 'dimple' (J_0 Bessel) and 3D ($\sin(kx) \times \sin(ky)$) interface perturbations (as opposed to the 2D sinusoidal corrugation in Fig. 3). We are also doing numerical simulations to investigate 2D-3D differences in SN 1987A. Fig. 7 illustrates a simple investigation, comparing the result of imposing 2D sinusoidal, dimple, and 3D velocity perturbations at the He-H interface after passage of the shock through the interface. The 3D bubble (Fig. 7c) grows faster than the 2D bubble (b), a result already anticipated from previous Nova experiments [29], and the spike grows $\approx$ 25% faster in 3D. The dimple spike

(b) grows significantly faster than the 2D spike. Fig. 7d shows the distribution by mass of the He velocities at 12,000 s, by which time the blast wave has exited the H layer. The broadening of the velocity profiles in the He layer (the H layer is $\approx$ 20% He by mass in the initial model) for the 3D and dimple perturbations is evident.

In the Nova experiments, we are comparing 3D ($\sin(kx) \times \sin(ky)$) interface perturbations to the 2D sinusoidal corrugation. The target consists of a 200 μm thick CHBr ablator of density 1.54 g/cm^3, backed by a thick layer of foam of density 100 mg/cm^3. We again use Nova in indirect drive, mounting the target on a window in the side of the hohlraum. We use PROMETHEUS to model the experiment, because, unlike our version of CALE, PROMETHEUS allows 3-dimensional geometries. We use only low resolution, 24 zones per half wavelength, because of the expense of the 3D simulations. For the 2D sinusoid, we use $\lambda = 200\,\mu$m, amd for the 3D 'crosshatch' we use $\lambda_x = \lambda_y = \sqrt{2} \times 200\,\mu$m. **[figure to be included showing target, similar to Omega figure, showing initial perturbations, snapshots of interface at 40 ns, and bubble and spike positions versus time.These figures or very similar ones have already been bluesheeted and presented at conferences.]** From the PROMETHEUS simulation, we find that the 3D spike grows about 35% faster than the 2D spike.

We will compare a Bessel dimple perturbation to the 2D sinusoid in the Omega experiments. The Omega shots will be done in direct drive, with the laser directly illuminating the target. The target will consist of 50 μm of CH_2 backed by 150 μm of CHBr, with a lighter layer of foam. The CH_2 layer facing the laser prevents preheating of subsequent layers by transmitted X-rays. We use CALE to simulate this experiment, since CALE has both planar and axially symmetric r-z geometry. The results of the simulation are shown in Fig. ??, with the shapes of the two interfaces at 40 ns, and the bubble and spike positions vs. time. The Bessel spike grows approximately 35% faster than the 2D

Fig. 6.— Indirect drive Nova SNRT 2D sine vs. 3D crosshatch. (a) 2D sinusoid; initial perturbation and interface at 40 ns. (b) Same for crosshatch. (c) Bubble and spike positions vs. time Note the greater penetration of the 3D spike.

spike.

6. Further work

We are also designing targets which incorporate more features of the actual star, in particular divergent geometry and multiple layers of different density. Among the effects we will study with these targets are the feedthrough of perturbations from one interface to the next. **[figure to be included showing target, and result of CALE simulation at 160 ns. These figures or very similar ones have already been bluesheeted and presented at conferences.]**

Work performed under the auspices of the U.S. Department of Energy by the Lawrence Livermore National Laboratory under contract number W-7405-ENG-48. D. A. and J. K. were supported in part by

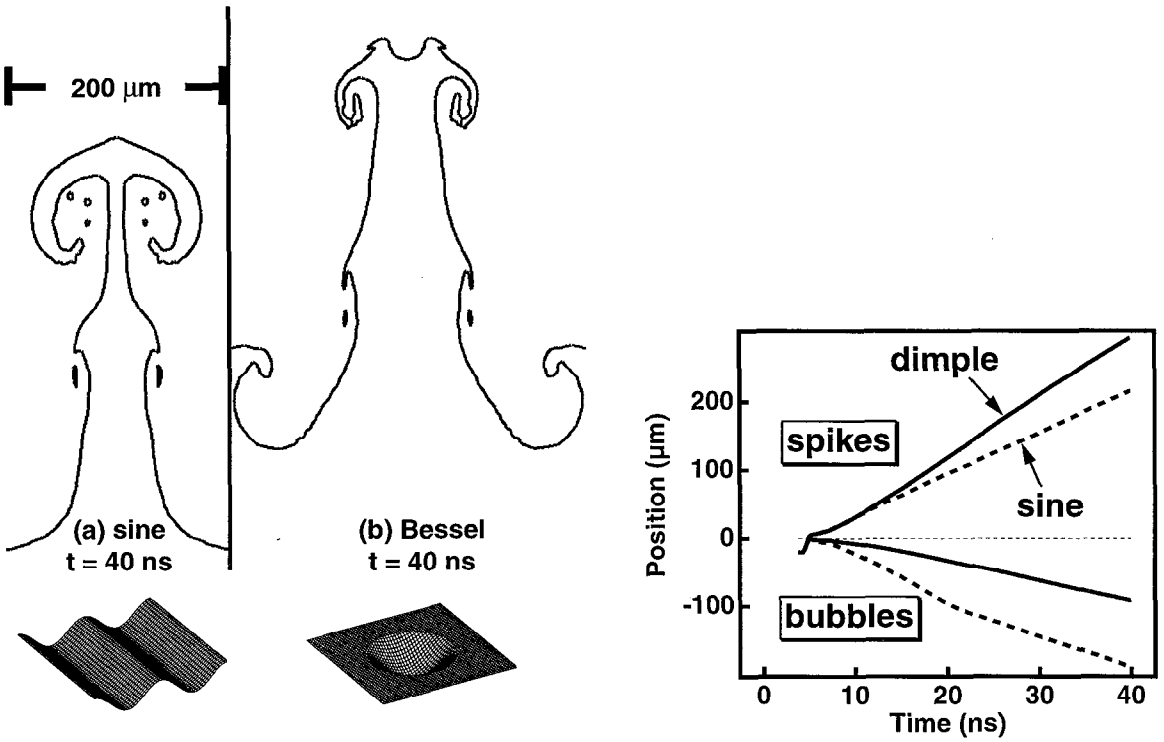

Fig. 7.— Direct drive SNRT 2D sine vs. dimple. (a) 2D sinusoid; initial perturbation and interface at 40 ns. (b) Same for Bessel dimple. (c) Bubble and spike positions vs. time Note the greater penetration of the Bessel spike.

NASA grant NAGW-2450 and NSF grant ASTRO 9015976.

REFERENCES

Kane J, Arnett D, Remington B A, Glendinning S G, Castor J, Wallace R, Rubenchik A, and Fryxell B A 1997 ApJ **478** L75

Richtmyer R D 1960 *Commun. Pure App. Math.* **13** 297

Meshkov E E 1969 *Izv. Akad. Nauk SSSR Mekh. Zhidk.* **Gaza 4** 151 [*Izv. Acad. Sci. USSR Fluid Dynamics* **4** 101 (1969)]

Lord Rayleigh 1900 Scientific Papers II 200 Cambridge, England

Taylor, Sir Geoffrey 1950 *Proc. R. Soc. London* **A201** 192

Arnett D, Bahcall J N, Kirshner R A and Woosley S E 1989 *Ann. Rev. A. Ap.* **27** 629

Shigeyama T and Nomoto K 1990 ApJ **360** 242

Hanuschik R W and Dachs J 1987 A&A **192** L29

Blanco V M *et al.* 1987 ApJ **320** 589

Witteborn F C, Bregman J D, Wooden D H, Pinto P A, Rank D M, Woosley S E and Cohen M 1989 ApJ **338** L9

Tueller J *et al.* 1990 ApJ **351** L41

McCray R 1993 *Ann. Rev. A. Ap.* **31** 175

Arnett D 1996 *Supernovae and Nucleosynthesis*, (Princeton: Princeton University Press)

Arnett D, Fryxell B and Müller E 1989 ApJ **341** L63

Fryxell B A, Müller E and Arnett D 1991 ApJ **367** 619

Müller E, Fryxell B A and Arnett D 1991 A&A **251** 505

Woodward P R and Colella P 1984 *J. Comp. Phys.* **54** 115

Glendinning S G 1992 *Rev. Sci. Instrum.* **63** 5108

Dionte G *et al.* 1996 *Phys. Plasmas* **3**, 614

Budil K S *et al.* 1996a Phys. Rev. Lett. **76** 4536

Peyser T A *et al.* 1995, Phys. Rev. Lett. **75** 2332

Larsen J T and Lane S M 1994 *J. Quant. Spect. Rad. Trans.* **51** 179

Barton R T 1985 In *Numerical Astrophysics*, ed. J. M. Centrella, J. M. LeBlanc and R. L. Bowers, Boston: Jones and Bartlett Publishers, Inc., pp. 482-497

Campbell E M, Holmes N C, Libby S B, Remington B A and Teller E 1997 *Laser and Particle Beams* **15** 607

Alon U, Hecht J, Ofer D and Shvarts D 1995 Phys. Rev. Lett. **74** 534

Hecht J, Alon U and Shvarts D 1994 *Phys. Fluids* **6** 4019

Alon U, Hecht J, Mukamel D and Shvarts D 1994 Phys. Rev. Lett. **72** 2867

Dahlburg J P, Gardner J H, Doolen G D and Hann S W 1993 *Phys. Fluids B* **5** 571

Marinak M M *et al.* 1995 Phys. Rev. Lett. **75** 3677

Rytuov *et al.*, submitted to Ap.J. (1998)

J. Fluid Mech **187** 353 (1988)

Thin shell approximation for g ~ 1/t

$$\ddot{x}(\xi,t) = -g(t)z' \qquad g(t) = \alpha/t$$
$$\ddot{z}(\xi,t) = g(t)x'$$

Assume a solution of the form

$$x(\xi,t) = \xi + f(t)\cos(k\xi)$$
$$z(\xi,t) = z_0(t) + f(t)\sin(k\xi)$$
$$\ddot{z}_0(,t) = g(t)$$

Then $\ddot{f}(t) - (k\alpha/t)f(t) = 0$ **and**

$$f(t) = \sqrt{\frac{t}{k\alpha}}\left\{a_1 \mathrm{I}_1(2\sqrt{[k\alpha t]}) - b_1 \mathrm{K}_1(2\sqrt{[k\alpha t]})\right\}$$

$$\dot{f}(t) = a_1 \mathrm{I}_0(2\sqrt{[k\alpha t]}) + b_1 \mathrm{K}_0(2\sqrt{[k\alpha t]})$$

The solution is a linear combination of the exponential and damped modified Bessel functions K_1 and I_1, with coefficients a_1 and b_1 with which we can fit the initial amplitude η_0 and velocity $d\eta/dt_0$ of the perturbation.

Thin shell analysis of SNRT

We take the initial conditions for Ott and potential flow (ie., η_0 and $d\eta/dt_0$) from the Mayer-Blewett theory of the RM instability:

$$\eta_0^* = \eta_0(1 - u_i / v_s)$$

$$\dot{\eta}_0 = \dot{\eta}_{0,\mathrm{MB}} = \frac{(\eta_0 + \eta_0^*)}{2} kA^* u_i$$

When we roughly account for decompression in the SNRT simulation, the thin shell result gives an upper bound on bubble position. SNRT growth should differ from this thin shell growth because for SNRT (a) the fluid above and below the thin shell is not massless and (b) λ = 200 μm and the thickness of the shell is h ~30-70 μm, giving λ/h ~ 3-6, whereas the thin shell theory is adequate for $\lambda/h > 2\pi$. As an *ad hoc* modification to the thin shell theory which crudely accounts for the massive fluids above and below, we can insert (without justification) the post-shock Atwood number A^* into the theory. Since $g = \alpha/t$, the classical, linear regime, semi-infinite layer growth rate is $\gamma(A^*,t) = (A^* kg)^{1/2} = (A^* k\alpha/t)^{1/2}$, and we get from the modified Ott theory the position and velocity functions:

$$f^*(t) = \sqrt{\frac{t}{A^* k\alpha}} \left\{ a_1 \mathrm{I}_1(2\sqrt{[A^* k\alpha t]}) - b_1 \mathrm{K}_1(2\sqrt{A^*[k\alpha t]}) \right\}$$

$$\dot{f}^*(t) = a_1 \mathrm{I}_0(2\sqrt{[A^* k\alpha t]}) + b_1 \mathrm{K}_0(2\sqrt{A^*[k\alpha t]})$$

Orig Fig

(a)

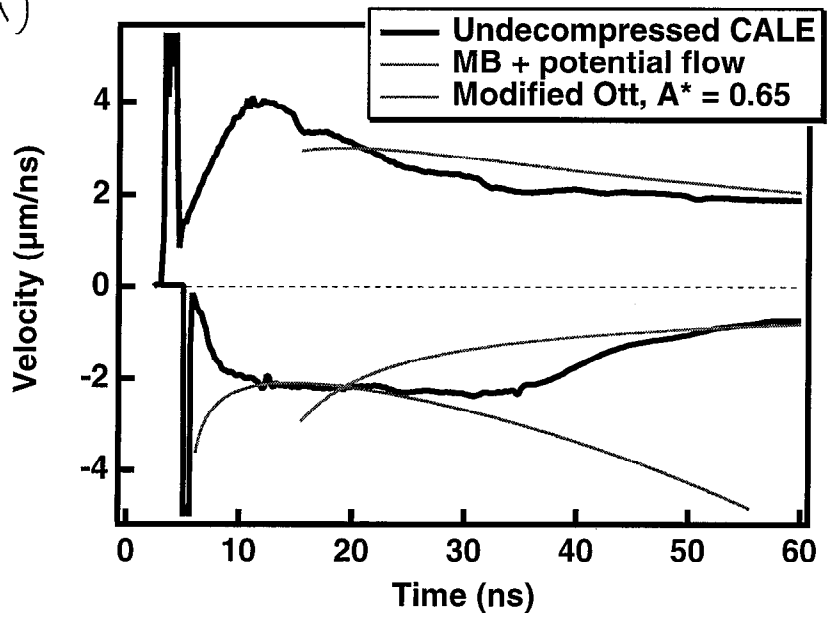

(b)

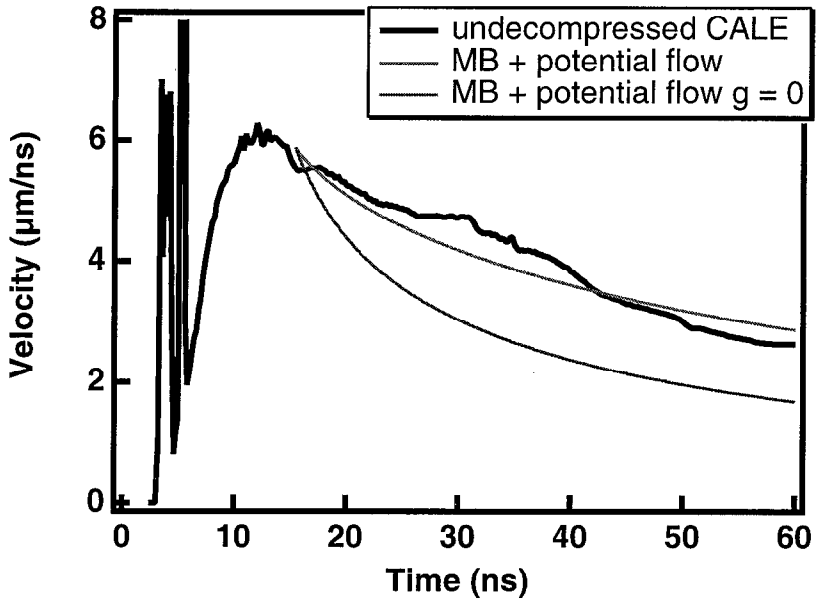

Jave Kane 10/1998

Jacobs Fig.

2D incompressible code tests

Jacobs
run 23
photo
t = 0.528 s

Reproduced from Fig. 4 (i, p. 408 of J W Jacobs & J M Sheeley, Phys. Fluids 8 (1996)

(a)

CALE 2D simulation
t = 0.528 s

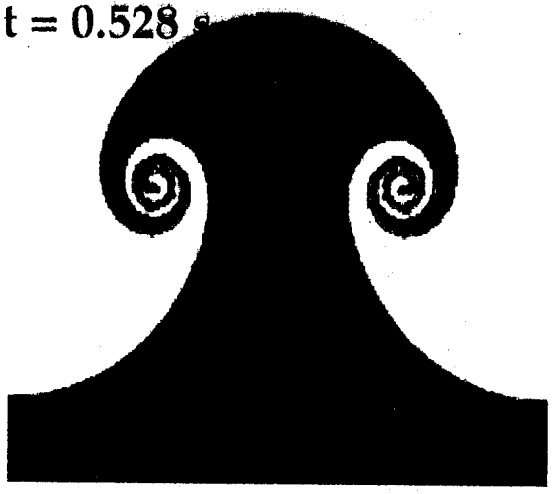

PROMETHEUS
2D simulation
t = 0.528 s

Jacobs experi-
ment schematic

Reproduced from Fig. 1 (i, p. 407 of J W Jacobs & J M Sheeley, Phys. Fluids 8 (1996)

(c)